DIELECTRIC AND MECHANICAL PROPERTIES OF NON-COVALENTLY FUNCTIONALIZED GRAPHENE NANOSHEETS (GNSs)/PDMS NANOCOMPOSITES

by

Yasin ALTIN

A thesis submitted in partial fulfillment of

the requirements for the degree of

Master of Science

(Materials Science)

at the

UNIVERSITY OF WISCONSIN–MADISON

2014

Abstract

Novel graphene nanosheets (GNSs)/poly(dimethylsiloxane) (PDMS) nanocomposites were fabricated using the non-covalent functionalization method. Their morphological, mechanical, and dielectric properties were evaluated. Pyrene–PDMS functional groups were utilized as functionalization agents to homogenously and efficiently disperse GNSs throughout the PDMS matrix. This non-covalent functionalization facilitated the dispersion of GNSs in the polymer matrix and also isolated the graphene layers to prevent their aggregation and formation of conductive pathways through the polymeric matrix. The dielectric properties of the GNSs/PDMS nanocomposites significantly improved with the addition of GNSs, which could be explained by the Maxwell–Wagnar–Sillars (MWS) effect and the microcapacitor model. With the incorporation of GNSs in the PDMS matrix (1.2 wt%), a dielectric constant 155 times larger than that of pure PDMS was obtained at 1 kHz, while a relatively low dielectric loss was preserved. The effect of the GNSs' concentration and functionalization ratios on the dielectric and mechanical properties were investigated. Moreover, the functionalization of GNSs increased the strain-at-break and decreased the tensile strength of the GNSs/PDMS nanocomposites.

Key Words: Polymer nanocomposite, dielectric elastomer, graphene, dielectric constant, pyrene–PDMS

1. INTRODUCTION

Polymeric nanocomposites with high dielectric permittivities are promising candidates for a wide range of applications including sensors for humidity, mechanical strain, and gases; artificial muscles and actuators; high-K gate dielectrics for flexible electronics; memory devices; super-capacitors for energy storage devices due to their flexibility; and light-weight, inexpensive, and convenient manufacturing processes [1-6]. Typical polymers inherently possess very low dielectric constants. However, their low dielectric constant can be significantly improved by incorporating various dielectric and conductive fillers [5, 7] such as ceramics (titanium dioxide (TiO_2)) [8], metals (such as silver) [9], high-dielectric-constant organic nanofillers (copper phthalocyanine oligomer (o-CuPc)) [10, 11] or conducting polymers (such as polyaniline) [12]. While the dielectric constant of polymers can be enhanced by these fillers, the increase typically requires high levels of filler loading, which can potentially lead to an increase in their weight and inferior mechanical and electrical properties such as significantly reduced flexibility and high dielectric loss [10, 13-17]. In addition, while conducting polymers can increase the dielectric constant of the insulating polymers, they may be chemically and thermally unstable due to doping [18-20].

In order to significantly reduce the electrical percolation threshold, and thus the required filler loading level in the polymer matrix, nanofillers with high aspect and surface-to-volume ratios are desirable [21]. In recent years, carbon-based nanofillers, such as carbon nanotubes (CNTs) and graphene nanosheets (GNSs), have drawn considerable attention due to their large aspect and surface-to-volume-ratios as well as a unique combination of mechanical, electrical, and thermal properties [22-26].

GNS is a one-atom-thick planar sheet of sp^2-bonded carbon atoms densely packed in a honeycomb crystal lattice [27]. GNS is the building block for all graphitic forms including 0-D buckeyballs and 1-D CNTs. A number of research groups, including ours, have reported that the addition of CNT can effectively increase the dielectric constant of CNT/polymer nanocomposites [6, 28-31]. A number of other studies have also found that graphene can improve the thermal and electrical conductivity of the polymer matrix [32, 33]. Even at low filler concentrations (below 2.5 vol%), the presence of GNSs causes significant improvements in mechanical, thermal, electrical, and dielectric properties of GNSs/polymer composites, because GNSs have high electrical and thermal conductivities, large aspect ratios, high surface-to-volume ratios and excellent mechanical properties [25, 26, 34].

Like any other type of polymer nanocomposites, in order to fully harness the potential benefits of graphene/polymer nanocomposites, it is essential to (1) disperse the GNSs uniformly in the polymer matrix, and (2) form desirable interfacial bonding. Although a number of graphene/polymer nanocomposites have been investigated, most of these studies used non-functionalized GNSs, thus limiting their effectiveness in enhancing a variety of material properties [32, 35, 36]. Poor dispersion can also lead to a higher electrical percolation threshold [37-40]. To improve their dispersion and interfacial interactions in the polymer nanocomposites, GNSs can be covalently functionalized. However, covalent functionalization of GNSs changes GNSs' electronic structure from sp^2 to sp^3 and subsequently causes a reduction in GNSs' electrical, thermal, and mechanical properties [41-46]. Therefore, it is hypothesized that the dielectric constant of the polymeric nanocomposites can be significantly improved if GNSs are properly functionalized via a non-covalent technique,

which will preserve GNSs' electronic structure thereby maintaining its excellent intrinsic electrical, thermal, and mechanical properties while also providing uniform dispersion and favorable interfacial interactions in the polymer matrix [47, 48]. Pyrene, a large aromatic compound, has a very similar electronic structure to graphene. In fact, pyrene can be defined as a cut piece from GNS [49-53]. As such, pyrene can be easily adsorbed onto the GNS and form remarkably strong interactions through π-stacking [54]. Previously, a number of pyrene-containing polymers have been prepared and utilized to functionalize CNTs in order to facilitate their dispersion in the polymer matrix [49-53]. However, reports on pyrene-containing polymer functionalized GNSs are still rare [55, 56]. The pyrene–poly(dimethylsiloxane) PDMS functionalized GNSs will retain the latter's excellent electrical conductivity thus effectively increasing the dielectric constant of the FGNS/PDMS nanocomposites. Moreover, pyrene–PDMS functionalized GNSs may also alleviate the reduction in the dielectric breakdown strength of the FGNS/PDMS nanocomposites caused by the incorporation of GNSs because the pyrene–PDMS polymer surfactant can effectively reduce the agglomeration of the GNSs [57].

In this study, pyrene-terminated poly(dimethylsiloxane) (i.e., pyrene–PDMS) was chosen to non-covalently functionalize the GNSs. The dielectric and mechanical properties of functionalized GNSs/PDMS nanocomposites and non-functionalized GNSs/PDMS nanocomposites were compared.

2. EXPERIMENTAL METHODS

Sylgard 184 PDMS base and curing agent were supplied from Dow Corning Corporation. Hydrochloric acid (37 wt%), poly(dimethylsiloxane) monohydroxy terminated

(Mn ~4670 g mol^{-1}), 1-pyrenebutyric acid, 4-(dimethylamino)pyridine, and phosphoric acid (85 wt%) were all obtained from Sigma-Aldrich. Graphite powder, sulfuric acid (98 wt%), methanol, and hydrazine monohydrate (>98 wt%) were obtained from Fisher Scientific, USA. Potassium permanganate, reagent ACS (+99 wt%), and N,N''-dicyclohexylcarbodiimide (99 wt%) were obtained from Acros Organics. Ethyl acetate (general use HPLC grade), hexane (general use HPLC grade), and dichloromethane (anhydrous) were obtained from Pharmco-Aaper. Tetrahydrofuran (ACS grade) was obtained from VWR. All chemicals were used without further purification.

2.1. Sample Preparation

2.1.1. Preparation of GONSs

In this study, graphene oxide nanosheets (GONSs) were prepared from graphite powder via an improved Hummer's method [58]. The improved Hummer's method possesses several advantages over the standard Hummer's method as toxic gases will not be generated during the reaction and the temperature can be easily controlled [58]. Briefly, 1g of graphite flakes and 6g of $KMnO_4$ were added into a 120 ml: 13.33 ml mixture of H_2SO_4/H_3PO_4 (9:1 volume ratio). The resulting mixture was stirred at 50°C for 12 h. Afterward, the mixture was cooled down to RT and then poured onto a mixture of 150 ml ice and 1 ml 30% H_2O_2. After filtration, the resulting solid was gradually washed and centrifuged with water, HCl, and ethanol, and the supernatant was decanted. Then, the resulting solid was washed several times with DI water until the solution pH was about 7. Finally, concentrated GONSs solution was frozen in liquid nitrogen and freeze-dried in a lyophilizer at a condenser temperature of–

87.0 ºC under vacuum (0.0014). The resulting low density graphene oxide powder was obtained after 5 days, then stored in a desiccator.

2.1.2. Preparation of GNSs

Hydrazine monohydrate was used as reducing agents for GONSs [59]. GONSs (400 mg) was loaded into a 50 ml centrifuge tube containing DI water (40 ml), and the concentrated mixture was sonicated (UP400S, hielscher USA) at 80% amplitude using a 3 mm probe in an ice-bath for 30 min. The concentrated mixture was decanted into a round bottom flask and DI water (360 ml) was added. After the mixture was additionally shaken, hydrazine monohydrate (4 ml, 98%, Aldrich) was subsequently added to the suspension and stirred with a stirring bar in an oil bath at 90 ºC under a water-cooled condenser for 24 h. After the reaction was completed, the solution was cooled down to room temperature and the final black solid product was washed with water (5x200 ml), methanol (5x200ml) and THF (3x100 ml). The GNSs were later stored in THF.

2.1.3. Synthesis of Pyrene–PDMS

Figure 1 shows the synthesis scheme of pyrene–PDMS. First, 1-pyrenebutyric acid powder was dissolved in dichloromethane (DCM) and then mixed with monohydroxy-terminated poly(dimethyl-siloxane) (PDMS–OH, molecular weight 5000 Da) at a 1:1 molar ratio in the presence of 4-dimethyl¬aminopyridine (DMAP) and N,N'-Dicyclohexyl-carbodiimide (DCC). The reaction mixture was stirred for 24 h, and the solid product was filtered. The filtrate was evaporated under reduced pressure. Subsequently, the residue was purified via silica gel column chromatography using ethyl acetate/hexane (1:9). The resultant

product was placed in a vacuum oven for drying at 30° C for 48 h. The chemical structure of pyrene–PDMS was characterized by nuclear magnetic resonance (NMR) and shown in Fig. 2. Peaks at 7.8 to 8.3 ppm were observed due to the protons on the aromatic ring of pyrene. The peaks at ~0.1 ppm were assigned to the methyl groups of PDMS. Ultimately, pyrene–PDMS provided better dispersion and favorable interfacial interactions in the silicone matrix [49-53].

2.1.4. Non-Covalent Functionalization of GNSs Using Pyrene–PDMS

Tetrahydrofuran (THF) was used as a polar solvent to prepare the non-functionalized GNSs/PDMS and functionalized GNSs/PDMS nanocomposites. First, a pyrene–PDMS/THF solution was prepared. GNSs were added to this solution and soaked overnight. The resulting pyrene–PDMS/GNSs/THF solution was sonicated for 80 min to allow pyrene–PDMS adsorption on the surfaces of the GNSs via π–π interaction.

2.1.5. Fabrication of Non-Functionalized and Pyrene–PDMS Functionalized GNSs/Silicone Nanocomposite Films

Dow Corning® Sylgard® 184 Silicone Elastomer Kit, a two-part silicone, was used as the polymer matrix in this study. Graphene suspension in THF was sonicated with a probe sonicator for 80 min.; then PDMS base was added to the suspension, and the resulting solution (PDMS/THF ratio 1 g:2 ml) was sonicated for 20 min. The curing agent (PDMS base/curing agent weight ratio 10:1) was added and the final solution was mixed by stirring. After the GNSs/silicone/THF solution was degassed under reduced pressure, non-functionalized GNSs/silicone nanocomposite films was prepared using the solution casting method as illustrated in Scheme 1 [60].

To prepare functionalized GNSs/silicone nanocomposite films, the silicone base was mixed directly into the homogenous pyrene–PDMS functionalized GNSs/THF solution by stirring and was sonicated for 20 min. The curing agent was added to the resulting GNSs/silicone/THF solution under vigorous stirring to produce a homogeneous GNSs/silicone/curing agent/THF solution. After degassing the resulting solution under reduced pressure, functionalized GNSs/silicone nanocomposite films were prepared using the solution casting method [60]. To study the effects of GNSs on the various material properties of FGNS/silicone nanocomposites films, loading levels ranging from 0 to 1.2 weight % were prepared.

2.2. Characterization

For each type of characterization described below, at least three specimens were measured for each sample and the average results were reported. Chemical structures of the GONS and GNS were characterized by a Bruker TENSOR series FTIR spectrometer and Thermo Scientific DXR Raman Microscope at a 532 nm laser excitation level at room temperature. The chemical structure of pyrene–PDMS was characterized by a Varian Mercury Plus 300 ^{1}H-NMR (300 HZ, DMSO-d_6). The microstructures of GNSs/PDMS film structures were investigated via a scanning electron microscope (SEM, LEO GEMINI 1530) with a field emission electron gun. The dielectric properties of the GNSs/PDMS nanocomposites were measured using an Agilent E4980A LCR meter at room temperature with an Agilent 16451B dielectric test fixture. The mechanical properties of these nanocomposites were characterized according to the ASTM standard for polymeric thin films (ASTM D882).

The breakdown voltages of the GNSs/PDMS nanocomposite films were measured using a Matsusada AMS-10B2 high voltage amplifier. At least three specimens were measured for each GNSs/PDMS nanocomposite film with varying GNS loading levels and varying functionalization ratios; the average results were reported. The bottom side of the nanocomposite film was electrically activated with carbon paste electrodes (CPEs) and the small region on the top side of the sample was activated. The electric field was applied to the system and the breakdown voltages were measured.

3. RESULTS AND DISCUSSION

3.1. Surface Chemistry of GNSs

Figure 3 shows the FT-IR spectrum of GONSs and GNSs. The characteristic features in the FT-IR spectrum of GONSs are the adsorption bands corresponding to the C=O (carboxylic acid) peak stretching from 1700 to 1740 cm^{-1} and the broad O–H peak stretching from 2500 to 3300 cm^{-1} [43]. After chemical reduction, these peaks decreased or disappeared which proves that the chemical structure of graphene was successfully restored by hydrazine hydrate.

Raman spectra (Fig. 4) of graphite, GONSs and GNSs significantly changed during the oxidation and chemical reduction process. The in-phase vibration of the graphite lattice (G band) at 1575 cm^{-1} and the (weak) disorder band caused by the graphite edges (D band) at approximately 1347 cm^{-1} were observed [61, 62]. Raman spectra of GONSs showed larger and wider D and G band (at 1345 cm^{-1} at 1583 cm^{-1}) and the G band shifted towards higher frequency due to the extensive oxidization [59] . The increase of the disorder degree in the graphite intercalation cause a broader G and D band [63]. The grain size of graphite

crystallite is inversely proportional to the D band intensity [63]. As shown in Fig. 4, when the G band of GONSs widens and the peak intensity decreases, the D band increase. This indicates that the oxidation process caused an increase in the number of oxygenated functional groups, which increased a number of defects and transitions of sp^2 carbon hybrid to sp^3 carbon hybrid [63]. Chemical reduction of GONSs resulted in reduced peak intensities for both D and G bands. Also the D/G intensity ratio increased compared to that of GONSs. This was the average scale of sp^2 hybrid is smaller than that of graphene oxide [59, 61]. Also new graphitic domains were created might be smaller in the size than ones present in GONS [59]. Both FTIR and Raman data confirmed that GONSs and GNSs successfully synthesized.

3.2. Morphological Properties of GNSs/PDMS Nanocomposites

The quality of GNS dispersion in the PDMS matrix directly correlates to the effectiveness of improving mechanical and dielectric properties of the GNSs/PDMS nanocomposites. The properties of composites are also intimately linked to the aspect ratios and surface-to volume ratios of the GNSs. As shown in Figure 5(a), the GNSs are dispersed homogeneously in the PDMS matrix. From Figure 5(b) it can be seen that the average lateral dimensions of the GNS appears to be higher than 1 μm, which is promising owing to the high aspect ratios of the sheets. Moreover, the GNSs dispersed in the composites appear to be crumpled and wrinkled which significantly affects the mechanical properties of the resulting nanocomposites as will be discussed later (c.f. Figure 2(b)).

Figure 6 (a-b) shows the microstructure of GNSs/PDMS nanocomposites before and after functionalization of GNSs. As can be seen in the images, the GNSs are homogeneously

dispersed in polymer matrices for both functionalized and non-functionalized GNSs/PDMS nanocomposites.

3.3. Dielectric Properties of GNSs/PDMS Nanocomposites

The dielectric properties of polymer nanocomposites are strongly affected by the type of polymer matrix, the nanoparticle characteristics (such as aspect ratio, surface-to-volume ratio, electrical conductivity, and loading level), the fabrication method, and the degree of nanoparticle dispersion in the polymer matrix [33, 64-68]. In this study, poly(dimethylsiloxane) (PDMS) was used as a polymer matrix with a very low dielectric constant of around 3, which is almost independent of frequency level. However, PDMS's low dielectric constant can be significantly improved by adding highly conductive nanoparticles such as GNSs, CNTs, etc.

For an electrically conductive filler/polymer composite, assuming the concentration of the conductive filler is *f*, the effective dielectric constant of the composite has been predicted to follow a critical pattern of behavior,

$$\varepsilon = \varepsilon_m \left\{ (f_c - f) \Big/ f_c \right\}^{-q} \qquad (1)$$

where ε_m is the dielectric constant of the insulating matrix, q is a critical exponent (~1 for a three-dimensional composite), and f_c is the electrical percolation threshold [8, 9, 69]. A dramatic increase in dielectric constant can be obtained as the concentration of conductive fillers approaches the percolation threshold. Physically, this phenomenon can be explained as follows. When the concentration of the conductive filler is close to the percolation threshold, a

large number of conductive GNSs are isolated by very thin insulating polymer layers within the nanocomposites, forming a network of nano/micro-capacitors, thereby dramatically increasing the dielectric constant of the nanocomposites [9]. In addition, Maxwell–Wagner–Sillars (MWS) polarization for heterogeneous systems also plays a very important role in enhancing the dielectric constant [5, 70, 71]. The MWS effect is associated with the entrapment of free charges at the interface of the insulating polymer and the conductive filler [5, 70, 71]. Therefore another way to increase dielectric constant at the same filler concentration is by obtaining a better conductive nanoparticle dispersion in the polymer matrix which increases interfacial areas [33]. Also, nanocomposites display a much higher dielectric constant at a lower frequency due to MWS polarization for heterogeneous systems [72].

The dielectric properties of pure PDMS and GNSs/PDMS nanocomposites at various frequencies ranging from 1 kHz to 2 GHz are shown in Figure 7. The dielectric constant was significantly increased by the addition of GNSs. For instance, with the addition of 1.2 wt% GNSs to the PDMS matrix, the dielectric constants of the GNSs/PDMS nanocomposites were 512 and 71 at 1 kHz and 100 kHz, respectively, which were 158 and 22.3 times higher than those of pure PDMS, respectively. These improvements are significantly higher than those previously reported for hydroxylated MWCNT/PDMS nanocomposites [6]. In the afore mentioned study, pristine and hydroxylated MWCNT was used as a filler for the PDMS matrix; the electrical and dielectrical properties of the 6 wt% $MWCNT_{pristine}$ composites were ~1554 and ~875 at 1 kHz and 10 kHz frequencies, respectively [6]. However, the dielectric loss also dramatically increased from ~0.003 for the pure PDMS to ~1.12 for the 1.2 wt% GNSs/PDMS nanocomposite (Fig. 8) at 1 kHz frequency.

Figure 9 and 10 show the dielectric properties of the GNSs/PDMS nanocomposites as a function of GNSs concentration (weight%) in PDMS from 0 to 1.2%. As the figures show, the dielectric constant and dielectric loss strongly depended on the GNSs concentration. The dielectric constant increased slightly until 0.2 wt% GNSs, and dramatically increased at the 0.5 wt% GNSs concentration. The addition of GNSs to the composite increased both the dielectric constant (Fig. 9) and the dielectric loss (Fig. 10). The dramatic increase in the dielectric constant at 0.5 wt% can be explained by the percolation theory as per Eq. (1). When f approaches f_c in Eq. (1), the dielectric constant becomes abnormally high.

The microcapacitor model accounts for the dramatic increase in the dielectric constant at the percolation threshold. This model describes how the conductive graphene layers act as two electrodes, while the thin PDMS layer in-between acts as a dielectric. GNSs' morphology and high surface-to-volume ratio, as well as its uniform dispersion in the PDMS matrix, play an important role in improving the dielectric performance of the microcapacitor networks [33, 73]. Moreover, previous research has reported that the dielectric properties can be improved by optimizing the fabrication methods of the nanocomposite films [64, 74].

As mentioned before, the functionalization of GNSs helps the dispersion of GNSs in the polymer matrix and also isolates the graphene layers to prevent a conductive path from forming. Moreover, one of the important advantages of the non-covalent functionalization of GNSs is that it does not change the electronic structure of the GNSs [75-77]. Pyrene, which resembles a piece cut from a graphene sheet, is electronically similar to graphene. Therefore, the interaction between graphene and pyrene is very similar to the interaction between two graphene layers [51]. Thus PDMS with pyrene anchor units was used as a non-covalent

functionalizer for GNSs. When non-conductive pyrene–PDMS surrounded each graphene layer, it helped the dispersion of GNSs but also decreased the conductivity of each GNSs in the PDMS matrix. 0.8 wt% GNSs were chosen as a model and functionalized with different pyrene-PDMS/GNSs weight ratio. As shown in Fig. 11 and 12, the functionalization of GNSs decreased the dielectric constant of the nanocomposite and also decreased the dielectric loss. For instance, when comparing non-functionalized and 1:4 pyrene–PDMS functionalized samples, the dielectric constant decreased from 411 to 306 at 1 kHz, respectively. Also the dielectric loss decreased from 1.31 to 0.95 for the same samples. The functionalization ratio effect on the dielectric constant and dielectric loss can be clearly seen in Figs. 13 and 14.

Dielectric strength is one of the most important dielectric properties [78]. The dielectric strengths of the nanocomposites for different GNSs concentrations and different functionalization ratios at room temperature are shown in Figs. 15 and 16. While the presence of the GNSs in the polymer matrix decreased the dielectric breakdown strength of the nanocomposite, the increase in functionalization ratio improved the dielectric breakdown strength. For example, as shown in Fig. 15, the dielectric breakdown strength of pure PDMS was around 70 MV/m, which was reduced to 12.5 MV/m for 0.8 wt% GNSs/PDMS nanocomposites due to the possible formation of conductive paths and the presence of a large leakage current [57, 72]. The occurrence of conductive GNSs in the PDMS matrix was the main reason for the reduction of the dielectric breakdown strength [79]. Also, possible defects and impurities (including residual solvent and trapped air bubbles in the hybrid films) might have caused the deterioration of the dielectric breakdown strength [79]. As shown in Fig. 16, the functionalization ratios of GNSs, and the dielectric breakdown strengths of the

nanocomposites, were directly proportional. For example, the 0.8 wt% non-functionalized sample's dielectric breakdown strength was 12.5 MV/m, but increased to 14.16 MV/m and 26.88 MV/m for 1:4 functionalized and 1:8 functionalized samples, respectively. The presence of the insulator pyrene–PDMS, which surrounded the conductive GNSs, as well as the non-covalent functionalization of the GNSs, possibly impeded the formation of conductive paths between GNSs and the subsequent current leakage [57, 72].

3.4. Mechanical Properties of GNSs/PDMS Nanocomposites

The effect of the incorporation of GNSs on the mechanical properties of GNSs/PDMS nanocomposites is shown in Figure 17. The tensile strength of GNSs/PDMS nanocomposites decreased with the addition of GNSs. Also, the elongation-at-break for pure PDMS was higher than most GNSs/PDMS nanocomposites, for the except 1.2% GNSs/PDMS nanocomposite. The significant reduction in the tensile strength might be due to the GNSs impeding the cross-linking process of the polymer [80]. On the other hand, the elongation-at-break for GNSs/PDMS nanocomposites increased by adding GNSs. Lu et al. recently reported that the percentage of elongation-at-break for epoxy nanocomposites filled with thermotropic liquid crystalline epoxy grafted graphene oxide (LCE-g-GO) increased with increasing LCE-g-GO content [81]. Monticelli et al, recently claimed that weak interactions between nanofillers and the polymer matrix might cause a plasticizing effect on the mechanical behaviors of the nanocomposite films [82].

The stress–strain behaviors of functionalized GNSs/PDMS nanocomposites are shown in Figure 18. The 0.8% GNSs/PDMS sample was chosen as a model and was functionalized with three different GNSs/pyrene–PDMS ratios 1:4, 1:8, and 1:12. The

amount of pyrene–PDMS was calculated as a part of the polymer matrix. As shown in the graph, the elongation-at-break for the functionalized GNSs/PDMS samples correspondingly improved as the functionalization ratio increased. As can be seen in Fig. 18, the strain-at-break increased directly while the tensile strength decreased inversely, with increasing the concentration of the pyrene–PDMS groups. For example, the tensile strength of the non-functionalized 0.8% GNSs/PDMS was about 1.6 MPa, while the tensile strength of the 1:4 functionalized GNSs/PDMS sample sharply decreased to about 0.6 MPa. It decreased further to about 0.17 MPa at the 1:12 functionalization ratio. This phenomenon might be due to the fact that pyrene–PDMS groups, which consist of shorter PDMS chains (compared to the main matrix), acted as plasticizing agents and also reduced the crosslinking density of the main matrix [83].

4. CONCLUSION

Non-functionalized and pyrene–PDMS non-covalently functionalized GNSs/PDMS nanocomposites were successfully fabricated via a solution casting method. The morphological, dielectric, and mechanical properties of the elastomeric films were studied. Adding GNSs significantly increased the dielectric constant of GNSs/PDMS nanocomposites; however, the dielectric loss increased and the dielectric strength decreased which are undesirable for dielectric elastomers. Therefore, GNSs were non-covalently functionalized with pyrene–PDMS to improve the dispersion of GNSs in the polymer matrix and subsequently enhance the dielectric constant and maintain the dielectric loss at relatively low values. As a result of functionalization, elastomeric films with high dielectric constants, high dielectric strength, and low dielectric losses was prepared. For instance, GNSs/PDMS

nanocomposites containing only 1.2% GNSs yielded a dielectric constant over 155 times larger than that of pure PDMS at 1 kHz while still preserving a relatively low dielectric loss. Moreover, a 1:4 functionalized sample had a 25% lower dielectric constant and loss, as well as a 13% higher dielectric strength. Furthermore, the incorporation of GNSs in the PDMS matrix decreased the tensile strength and increased the elongation-at-break. These flexible high dielectric GNSs/PDMS nanocomposites are potential materials for flexible electronics and high-storage capacitors.

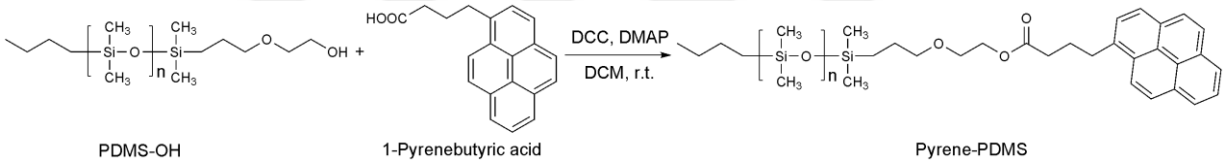

Figure 1 Synthesis scheme of pyrene–PDMS.

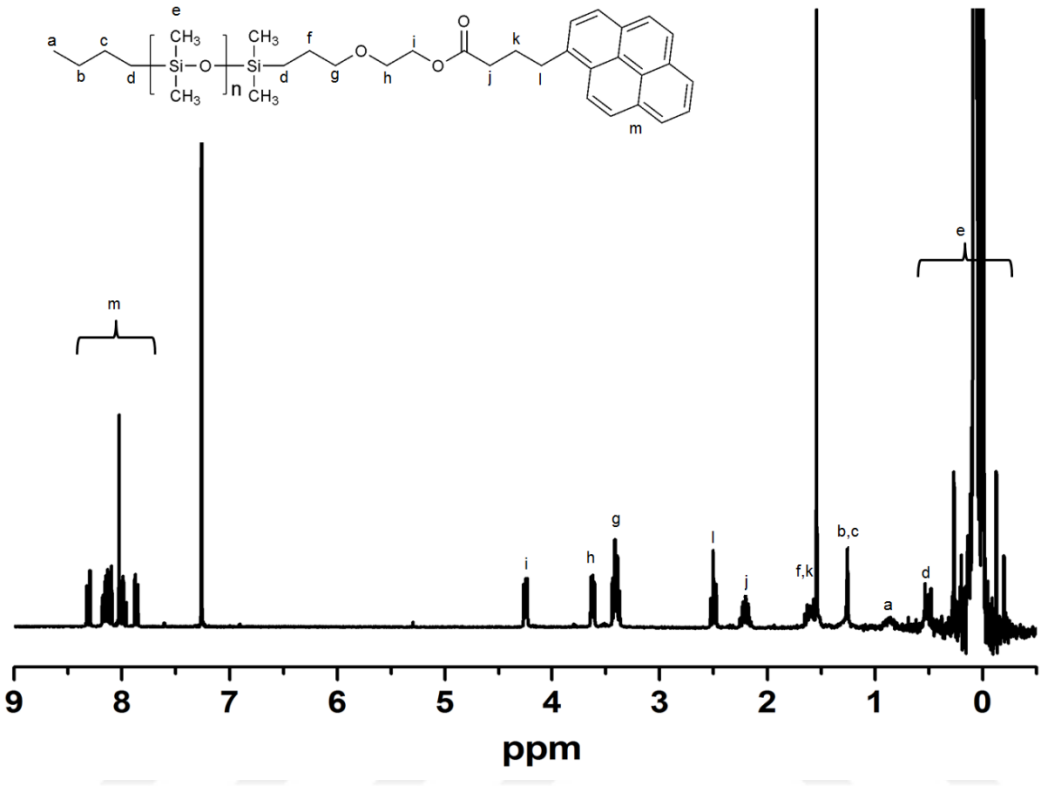

Figure 2. NMR results of pyrene–PDMS

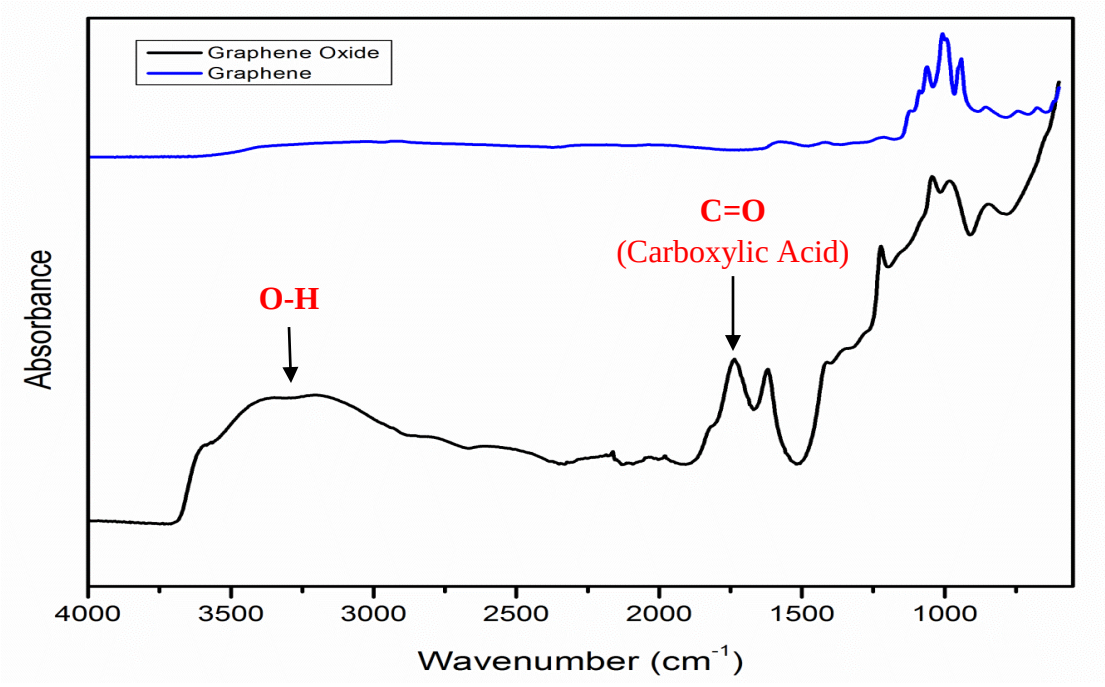

Figure 3. FT-IR results of graphite, GONSs and GNSs.

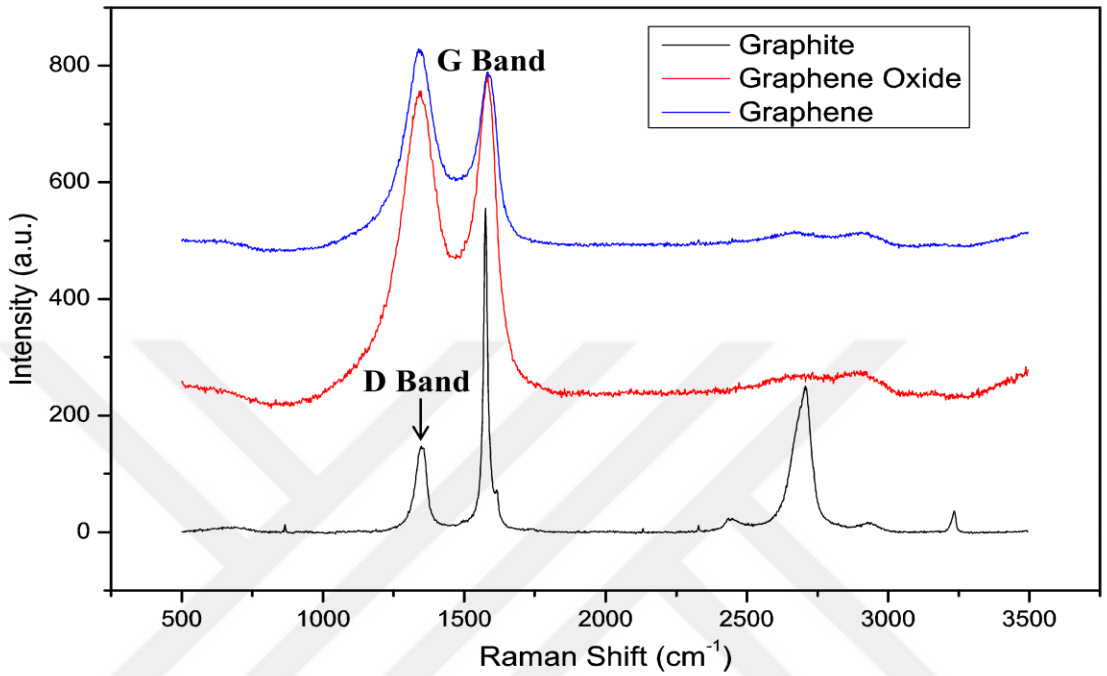

Figure 4. Raman spectrum of graphite, GONSs and GNSs**.**

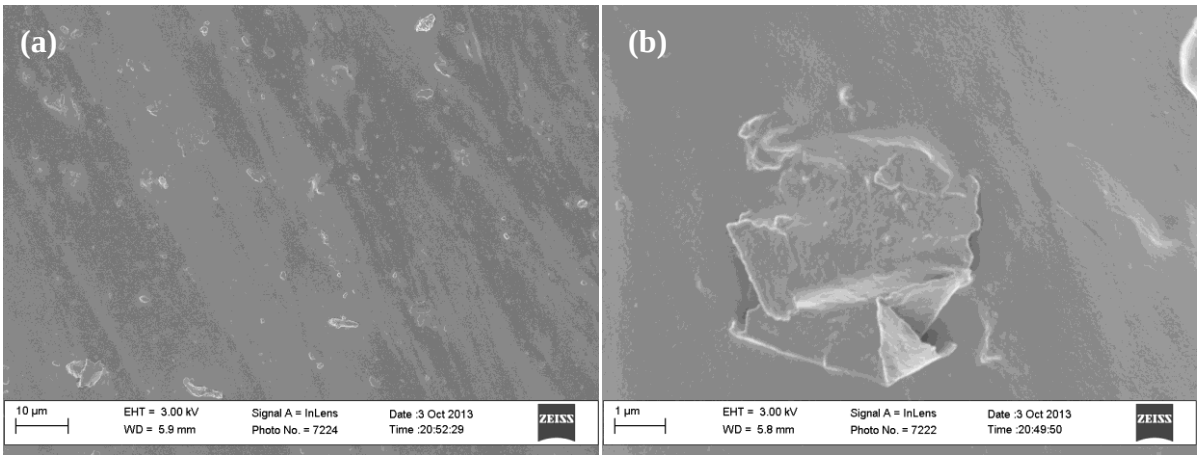

Figure 5. SEM images of GNSs/PDMS nanocomposites with scale bar (the concentration of GNS is 0.8 wt %) **(a)** 10 µm and, (**b)** 1 µm.

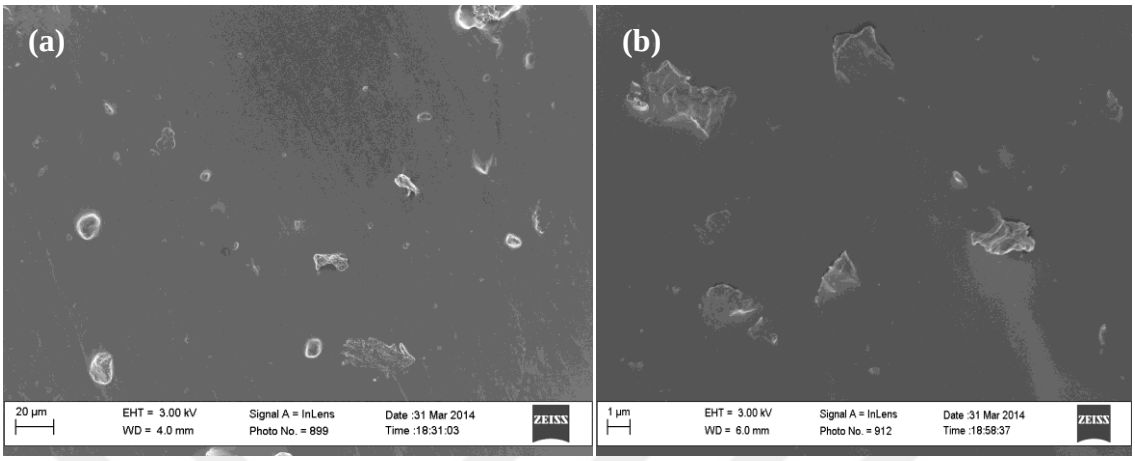

Figure 6. GNSs/PDMS nanocomposite; **(a)** functionalized and, **(b)** non-functionalized.

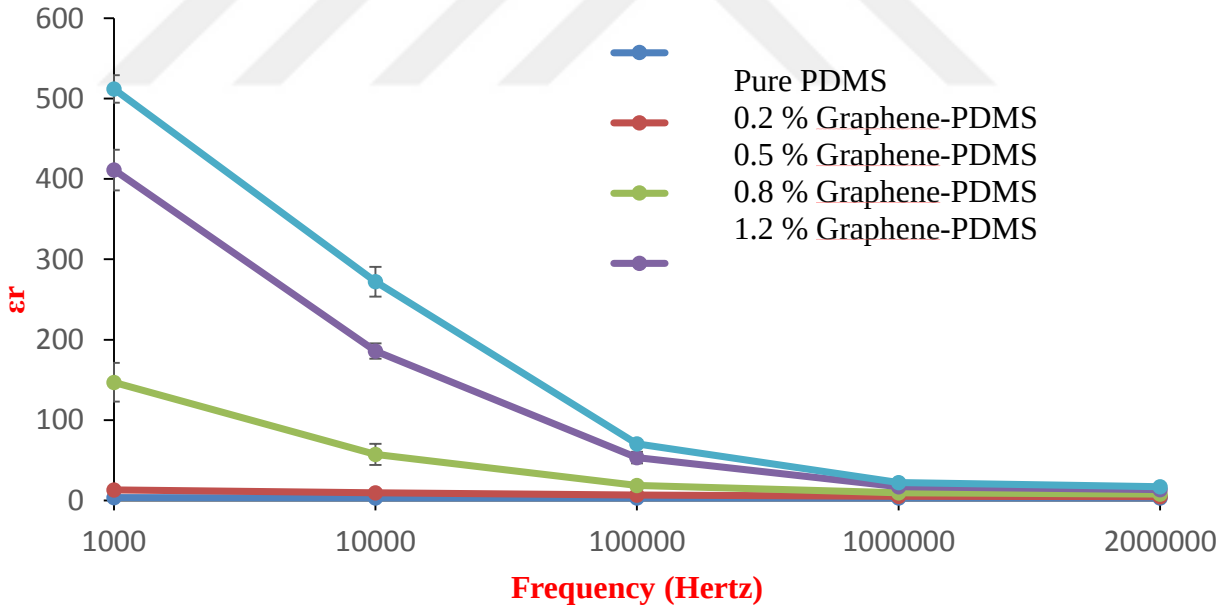

Figure 7. Dielectric constant of non-functionalized samples as a function of frequency.

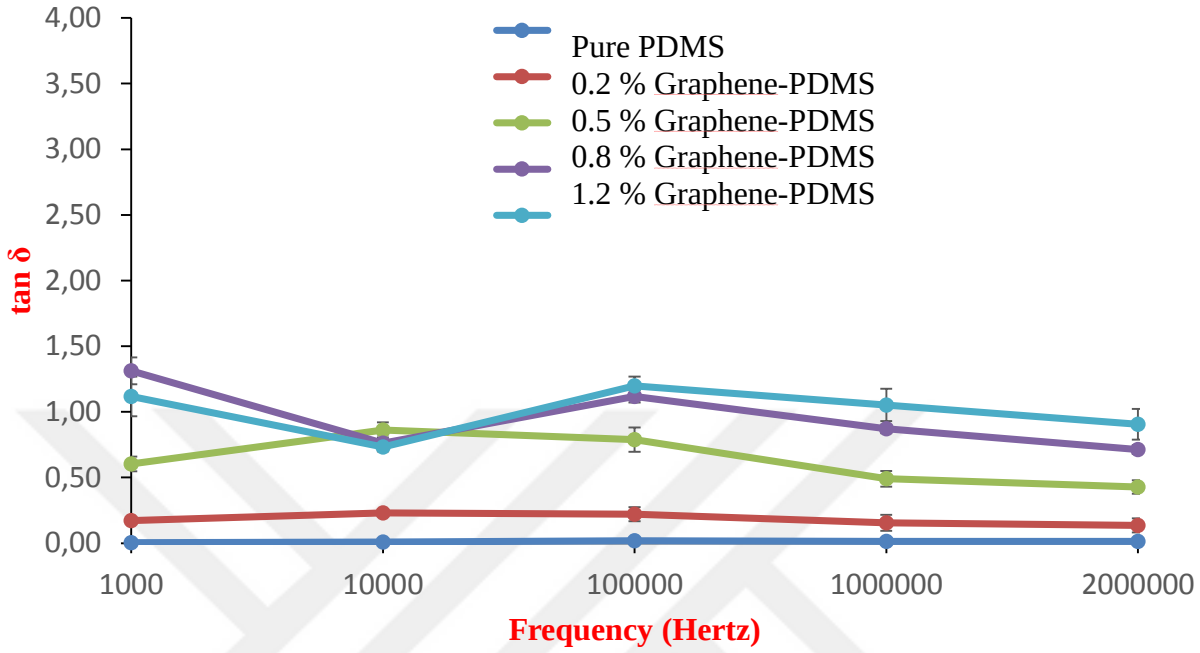

Figure 8. Dielectric loss of non-functionalized samples as a function of frequency.

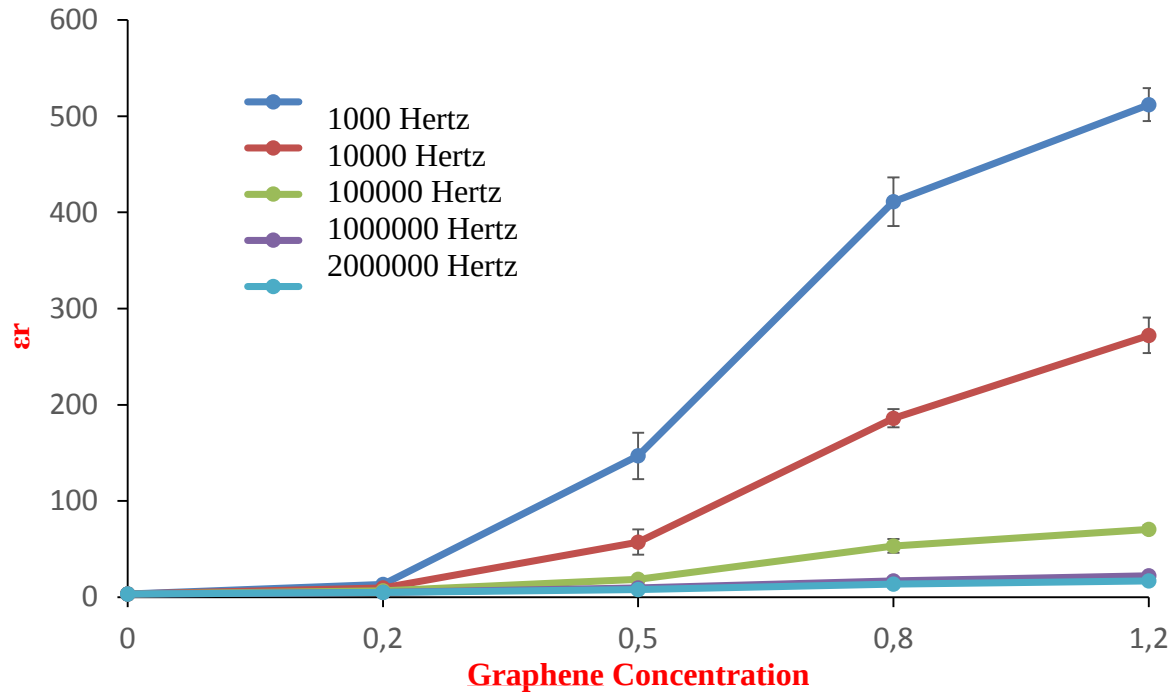

Figure 9. Dielectric constant of non-functionalized samples as a function of GNSs concentration.

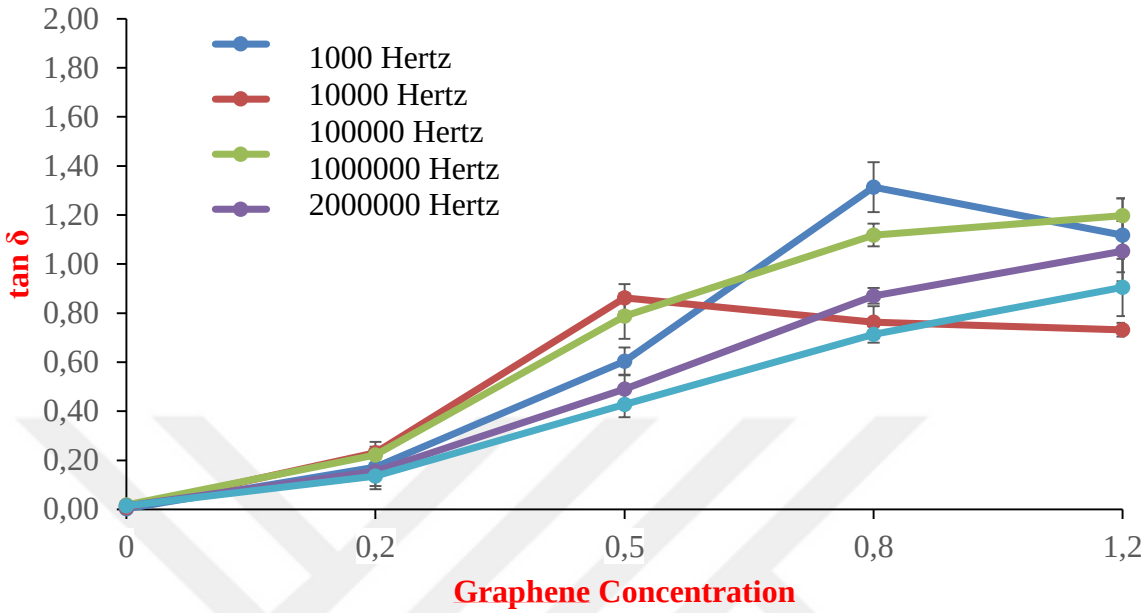

Figure 10. Dielectric loss of non-functionalized samples as a function of GNSs concentration.

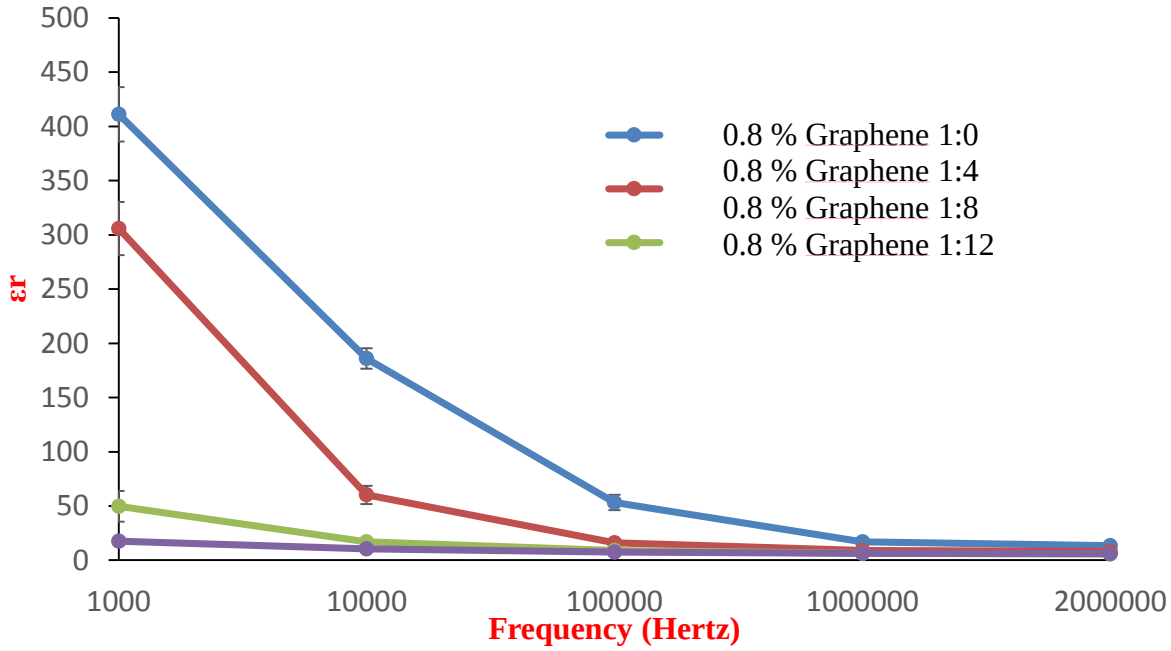

Figure 11. Dielectric constant of pyrene–PDMS functionalized samples as a function of frequency.

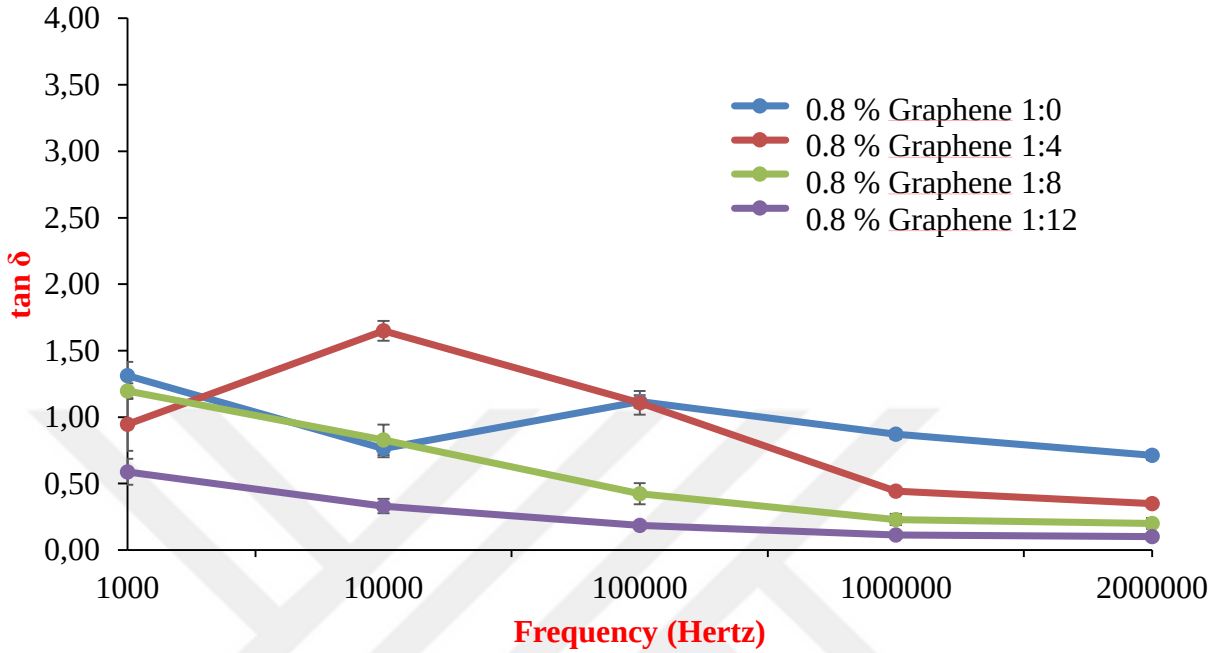

Figure 12. Dielectric loss of pyrene–PDMS functionalized samples as a function of frequency.

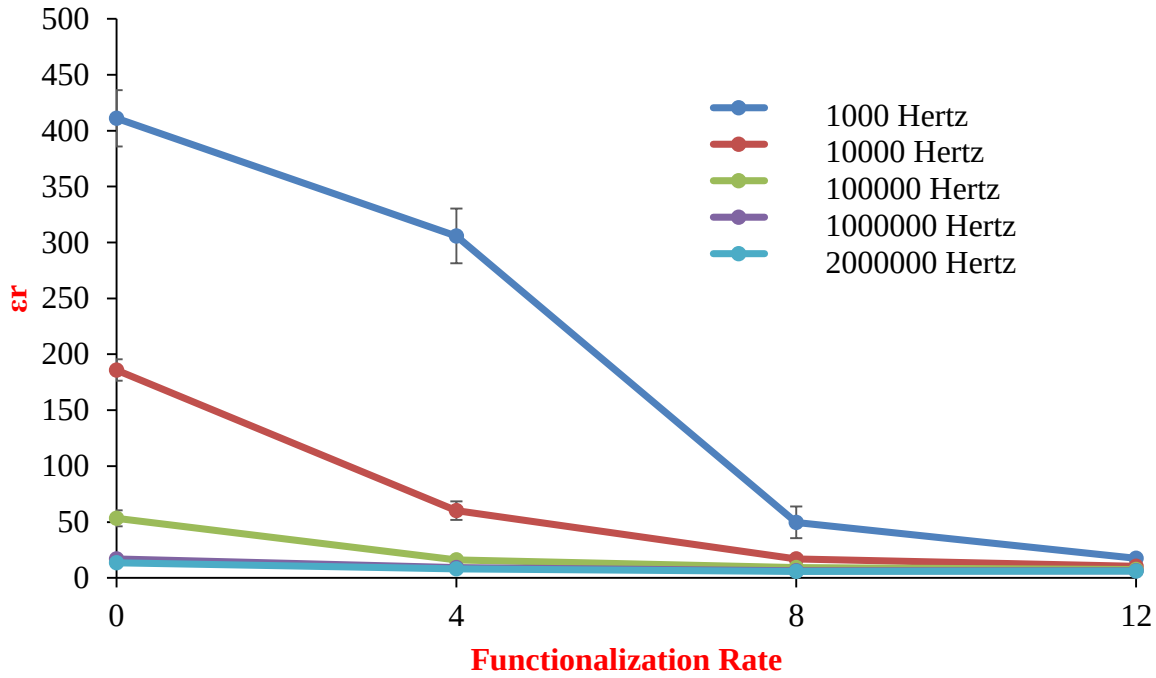

Figure 13. Dielectric constant of pyrene–PDMS functionalized samples as a function of functionalization rate

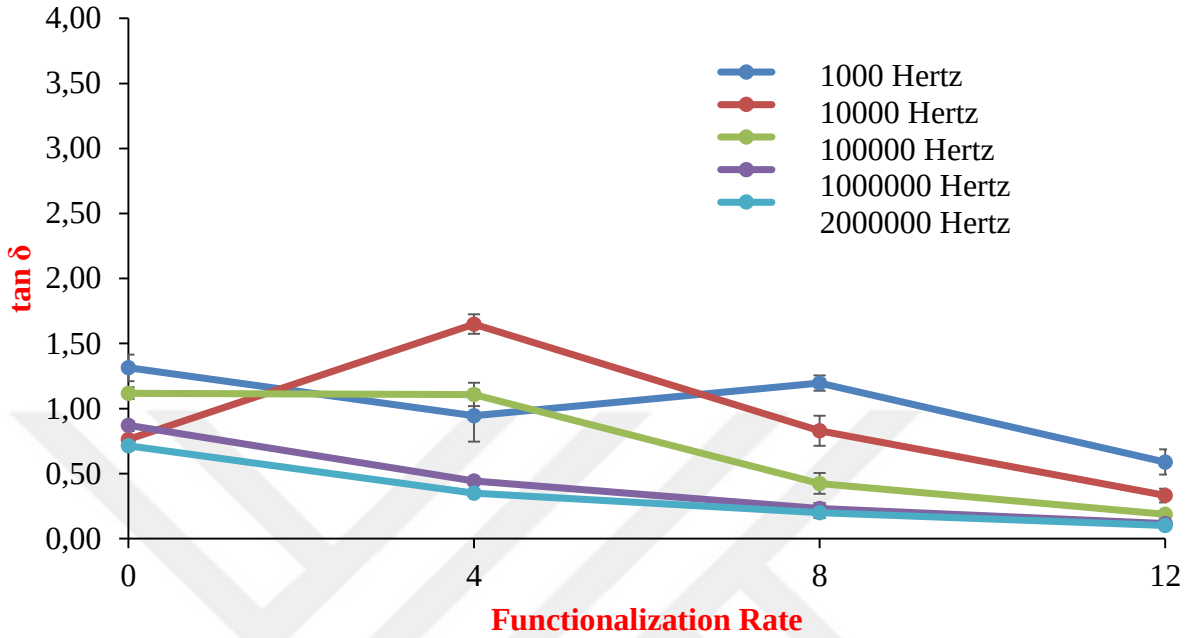

Figure 14. Dielectric loss of pyrene–PDMS functionalized samples as a function of functionalization rate.

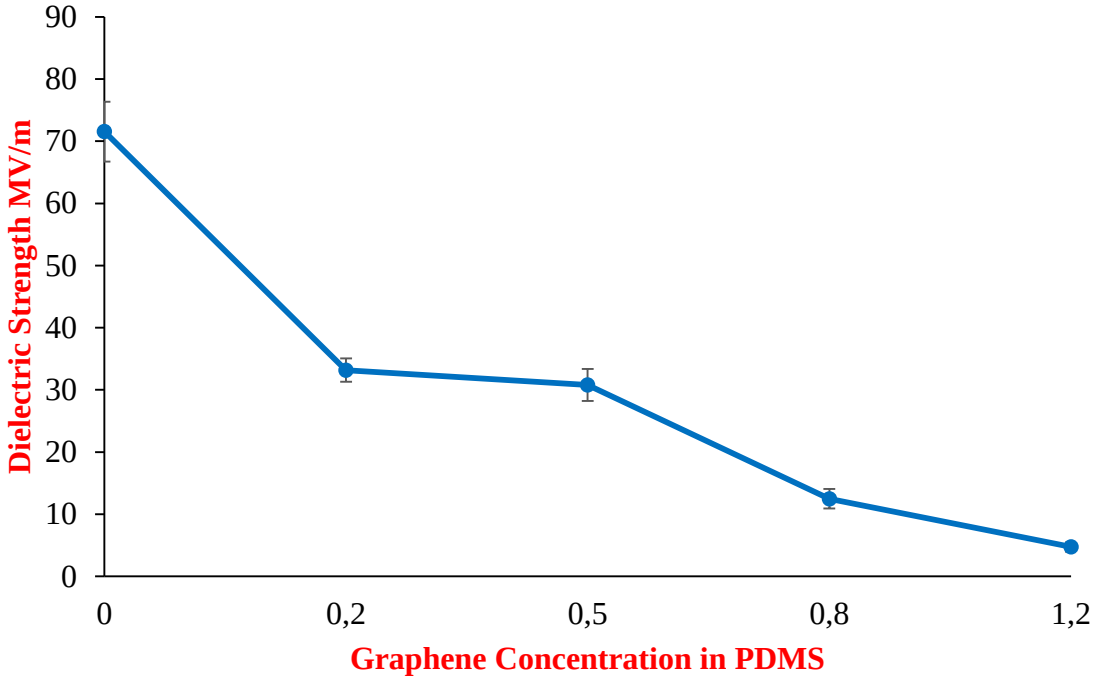

Figure 15. Dielectric strength of non-functionalized samples as a function of GNSs concentration.

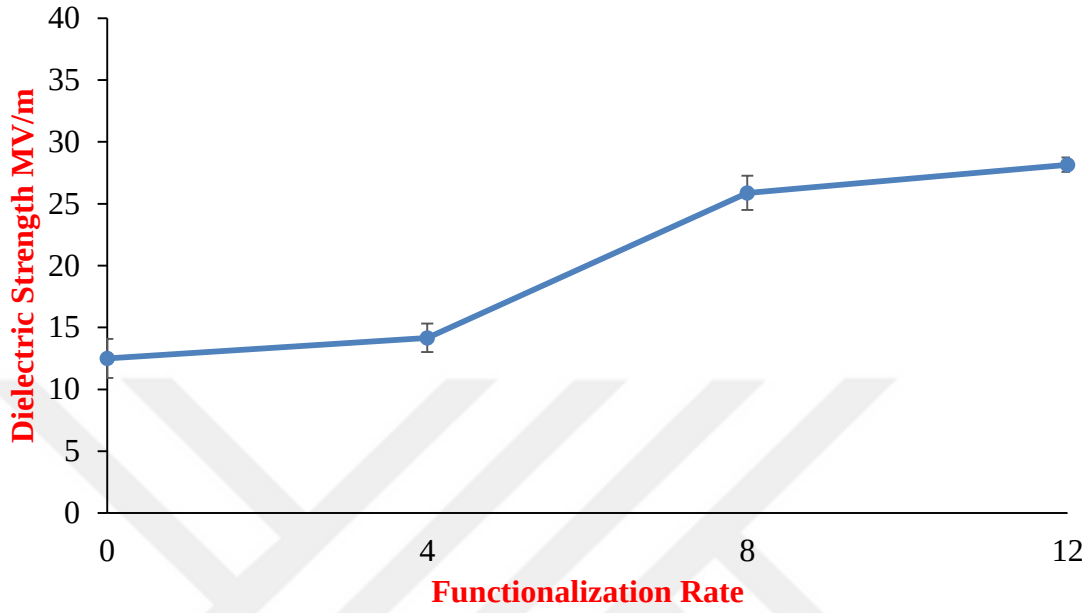

Figure 16. Dielectric strength of pyrene–PDMS functionalized samples as a function of functionalization rate.

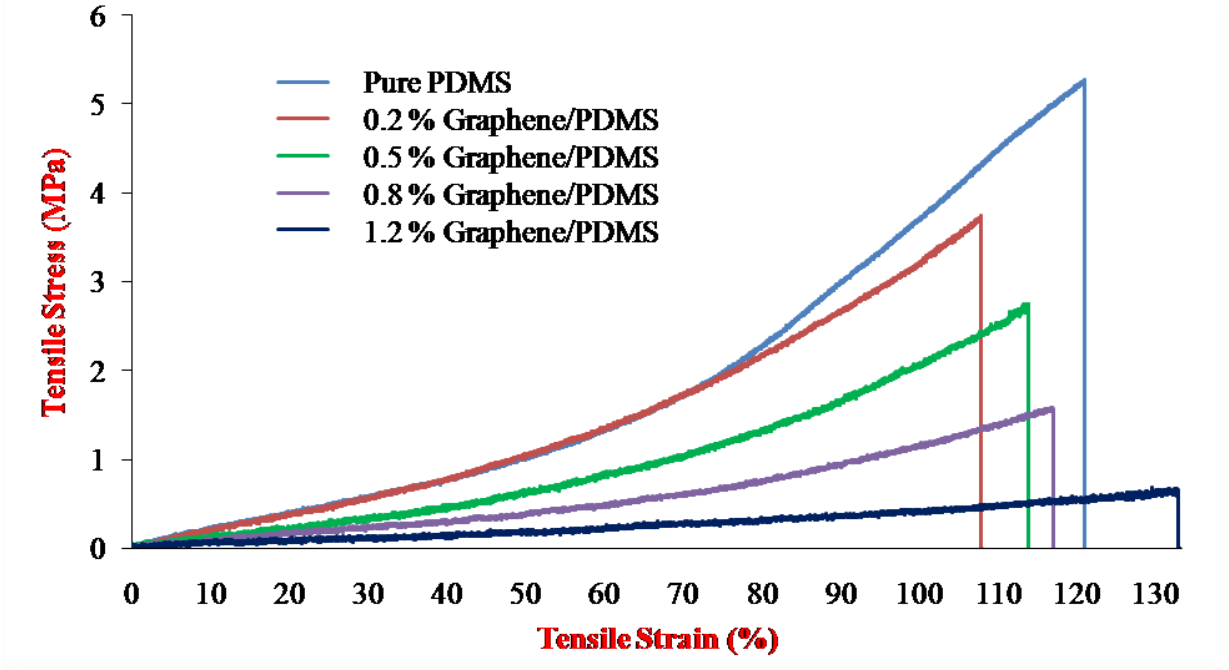

Figure 17. Stress–strain curve of non-functionalized samples.

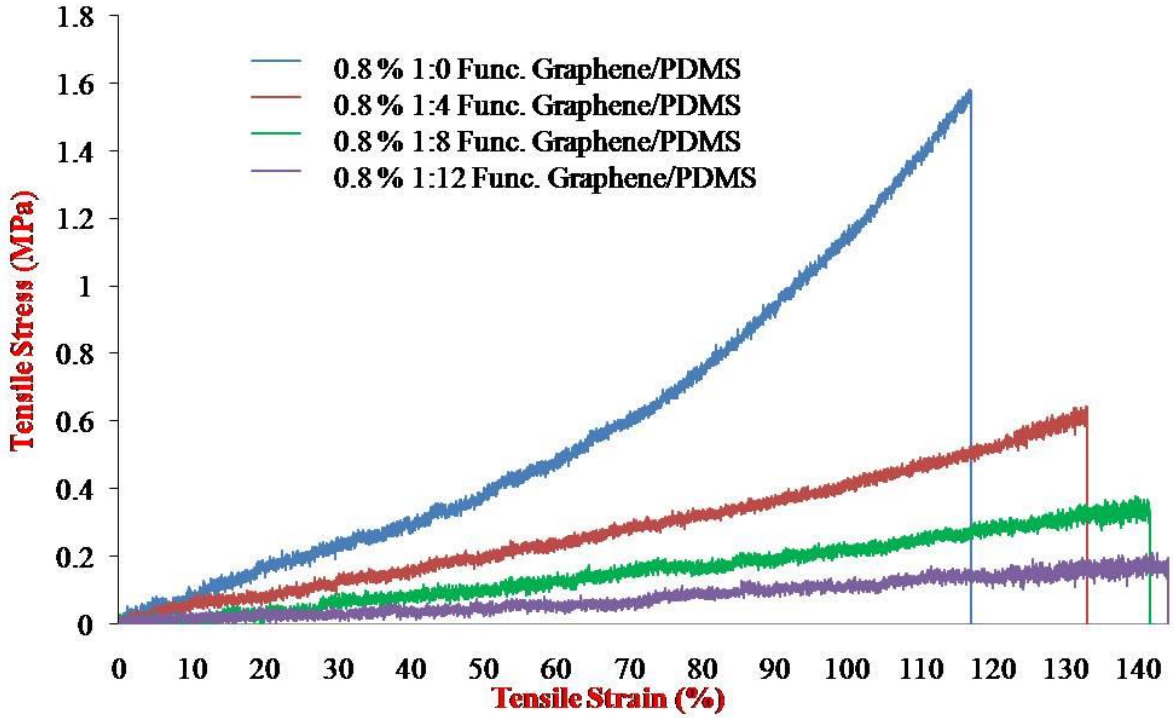

Figure 18. Stress–strain curve of functionalized samples.

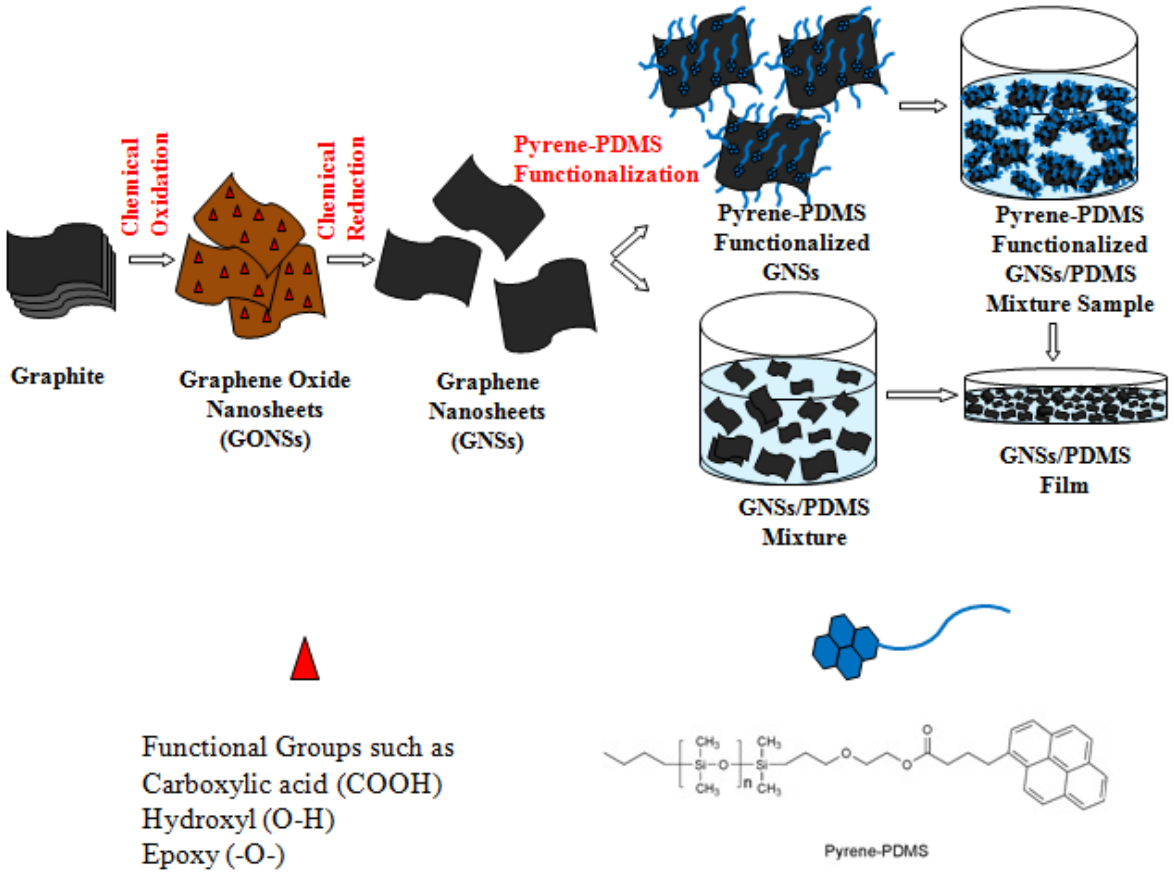

Scheme 1. Schematic diagram for GNS/PDMS nanocomposite film

References

[1] P. Brochu and Q. B. Pei, "Advances in Dielectric Elastomers for Actuators and Artificial Muscles," *Macromolecular Rapid Communications,* vol. 31, pp. 10-36, Jan 4 2010.

[2] R. Li, C. X. Xiong, D. L. Kuang, L. J. Dong, Y. A. Lei, J. L. Yao*, et al.*, "Polyamide 11/poly(vinylidene fluoride) blends as novel flexible materials for capacitors," *Macromolecular Rapid Communications,* vol. 29, pp. 1449-1454, Sep 1 2008.

[3] C. Wu, X. Y. Huang, X. F. Wu, L. Y. Xie, K. Yang, and P. K. Jiang, "Graphene oxide-encapsulated carbon nanotube hybrids for high dielectric performance nanocomposites with enhanced energy storage density," *Nanoscale,* vol. 5, pp. 3847-3855, 2013.

[4] J. M. Lu, K.S.; Wong C. P. . (2007) High-k Polymer Nanocomposites as Gate Dielectrics for Organic Electronics Applications. [Conference Paper].

[5] Z. M. Dang, L. Wang, Y. Yin, Q. Zhang, and Q. Q. Lei, "Giant dielectric permittivities in functionalized carbon-nanotube/electroactive-polymer nanocomposites," *Advanced Materials,* vol. 19, pp. 852-+, Mar 19 2007.

[6] R. R. Kohlmeyer, A. Javadi, B. Pradhan, S. Pilla, K. Setyowati, J. Chen*, et al.*, "Electrical and Dielectric Properties of Hydroxylated Carbon Nanotube-Elastomer Composites," *Journal of Physical Chemistry C,* vol. 113, pp. 17626-17629, Oct 15 2009.

[7] H. Stoyanov, M. Kollosche, D. N. McCarthy, and G. Kofod, "Molecular composites with enhanced energy density for electroactive polymers," *Journal of Materials Chemistry,* vol. 20, pp. 7558-7564, 2010.

[8] F. Carpi and D. De Rossi, "Improvement of electromechanical actuating performances of a silicone dielectric elastomer by dispersion of titanium dioxide powder," *Ieee Transactions on Dielectrics and Electrical Insulation,* vol. 12, pp. 835-843, Aug 2005.

[9] Y. Rao and C. P. Wong, "A novel ultra high dielectric constant epoxy silver composite for embedded capacitor application," in *Advanced Packaging Materials, 2002. Proceedings. 2002 8th International Symposium on*, 2002, pp. 243-248.

[10] Q. M. Zhang, H. F. Li, M. Poh, F. Xia, Z. Y. Cheng, H. S. Xu*, et al.*, "An all-organic composite actuator material with a high dielectric constant," *Nature,* vol. 419, pp. 284-287, Sep 19 2002.

[11] C. Huang, Q. M. Zhang, J. Y. Li, and M. Rabeony, "Colossal dielectric and electromechanical responses in self-assembled polymeric nanocomposites," *Applied Physics Letters,* vol. 87, p. 182901, Oct 31 2005.

[12] J. Y. Li, C. Huang, and Q. M. Zhang, "Enhanced electromechanical properties in all-polymer percolative composites," *Applied Physics Letters,* vol. 84, pp. 3124-3126, Apr 19 2004.

[13] J. Li, "Exchange Coupling in P(VDF-TrFE) Copolymer Based All-Organic Composites with Giant Electrostriction," *Physical Review Letters,* vol. 90, p. 217601, 2003.

[14] C. Huang, Q. M. Zhang, and J. Su, "High-dielectric-constant all-polymer percolative composites," *Applied Physics Letters,* vol. 82, pp. 3502-3504, May 19 2003.

[15] Z. M. Dang, Y. H. Lin, and C. W. Nan, "Novel Ferroelectric Polymer Composites with High Dielectric Constants," *Advanced Materials,* vol. 15, pp. 1625-1629, 2003.

[16] Z. M. Dang, J. K. Yuan, J. W. Zha, T. Zhou, S. T. Li, and G. H. Hu, "Fundamentals, processes and applications of high-permittivity polymer matrix composites," *Progress in Materials Science,* vol. 57, pp. 660-723, May 2012.

[17] Y. Bai, Z. Y. Cheng, V. Bharti, H. S. Xu, and Q. M. Zhang, "High-dielectric-constant ceramic-powder polymer composites," *Applied Physics Letters,* vol. 76, pp. 3804-3806, Jun 19 2000.

[18] H. Shirakawa, "The discovery of polyacetylene film: The dawning of an era of conducting polymers (Nobel lecture)," *Angewandte Chemie-International Edition,* vol. 40, pp. 2575-2580, 2001.

[19] A. G. MacDiarmid, ""Synthetic Metals": A Novel Role for Organic Polymers (Nobel Lecture)," *Angewandte Chemie International Edition,* vol. 40, pp. 2581-2590, 2001.

[20] A. J. Heeger, "Semiconducting and Metallic Polymers: The Fourth Generation of Polymeric Materials (Nobel Lecture)," *Angewandte Chemie International Edition,* vol. 40, pp. 2591-2611, 2001.

[21] C. W. Nan, "Physics of Inhomogeneous Inorganic Materials," *Progress in Materials Science,* vol. 37, pp. 1-116, 1993.

[22] X.-L. Xie, Y.-W. Mai, and X.-P. Zhou, "Dispersion and alignment of carbon nanotubes in polymer matrix: A review," *Materials Science and Engineering: R: Reports,* vol. 49, pp. 89-112, 2005.

[23] D. Tasis, N. Tagmatarchis, A. Bianco, and M. Prato, "Chemistry of Carbon Nanotubes," *Chemical Reviews,* vol. 106, pp. 1105-1136, 2006.

[24] Y. W. Zhu, S. Murali, W. W. Cai, X. S. Li, J. W. Suk, J. R. Potts*, et al.*, "Graphene and Graphene Oxide: Synthesis, Properties, and Applications," *Advanced Materials,* vol. 22, pp. 3906-3924, Sep 15 2010.

[25] S. Park, J. An, J. W. Suk, and R. S. Ruoff, "Graphene-Based Actuators," *Small,* vol. 6, pp. 210-212, Jan 18 2010.

[26] O. C. Compton and S. T. Nguyen, "Graphene Oxide, Highly Reduced Graphene Oxide, and Graphene: Versatile Building Blocks for Carbon-Based Materials," *Small,* vol. 6, pp. 711-723, Mar 22 2010.

[27] W. Choi, I. Lahiri, R. Seelaboyina, and Y. S. Kang, "Synthesis of Graphene and Its Applications: A Review," *Critical Reviews in Solid State and Materials Sciences,* vol. 35, pp. 52-71, 2010.

[28] C. Yang, Y. Lin, and C. W. Nan, "Modified carbon nanotube composites with high dielectric constant, low dielectric loss and large energy density," *Carbon,* vol. 47, pp. 1096-1101, 2009.

[29] Q. Li, Q. Xue, L. Hao, X. Gao, and Q. Zheng, "Large dielectric constant of the chemically functionalized carbon nanotube/polymer composites," *Composites Science and Technology,* vol. 68, pp. 2290-2296, 2008.

[30] L. Wang and Z. M. Dang, "Carbon nanotube composites with high dielectric constant at low percolation threshold," *Applied Physics Letters,* vol. 87, Jul 2005.

[31] S. Zhang, N. Zhang, C. Huang, K. Ren, and Q. M. Zhang, "Microstructure and Electromechanical Properties of Carbon Nanotube/ Poly(vinylidene fluoride—trifluoroethylene—chlorofluoroethylene) Composites," *Advanced Materials,* vol. 17, pp. 1897-1901, 2005.

[32] T. Kuilla, S. Bhadra, D. H. Yao, N. H. Kim, S. Bose, and J. H. Lee, "Recent advances in graphene based polymer composites," *Progress in Polymer Science,* vol. 35, pp. 1350-1375, Nov 2010.

[33] A. Javadi, Y. L. Xiao, W. J. Xu, and S. Q. Gong, "Chemically modified graphene/P(VDF-TrFE-CFE) electroactive polymer nanocomposites with superior electromechanical performance," *Journal of Materials Chemistry,* vol. 22, pp. 830-834, 2012.

[34] Y. W. Zhu, S. Murali, W. W. Cai, X. S. Li, J. W. Suk, J. R. Potts*, et al.*, "Graphene and Graphene Oxide: Synthesis, Properties, and Applications (vol 22, pg 3906, 2010)," *Advanced Materials,* vol. 22, pp. 5226-5226, Dec 7 2010.

[35] H. Kim, A. A. Abdala, and C. W. Macosko, "Graphene/Polymer Nanocomposites," *Macromolecules,* vol. 43, pp. 6515-6530, Aug 24 2010.

[36] R. Sengupta, M. Bhattacharya, S. Bandyopadhyay, and A. K. Bhowmick, "A review on the mechanical and electrical properties of graphite and modified graphite reinforced polymer composites," *Progress in Polymer Science,* vol. 36, pp. 638-670, May 2011.

[37] G. H. Chen, D. J. Wu, W. G. Weng, and W. L. Yan, "Preparation of polymer/graphite conducting nanocomposite by intercalation polymerization," *Journal of Applied Polymer Science,* vol. 82, pp. 2506-2513, Dec 5 2001.

[38] Y. H. She, G. H. Chen, and D. J. Wu, "Fabrication of polyethylene/graphite nanocomposite from modified expanded graphite," *Polymer International,* vol. 56, pp. 679-685, May 2007.

[39] Y. F. Zhao, M. Xiao, S. J. Wang, X. C. Ge, and Y. Z. Meng, "Preparation and properties of electrically conductive PPS/expanded graphite nanocomposites," *Composites Science and Technology,* vol. 67, pp. 2528-2534, Sep 2007.

[40] G. H. Chen, X. F. Chen, H. Q. Wang, and D. J. Wu, "Dispersion of graphite nanosheets in polymer resins via masterbatch technique," *Journal of Applied Polymer Science,* vol. 103, pp. 3470-3475, Mar 15 2007.

[41] K. A. Worsley, P. Ramesh, S. K. Mandal, S. Niyogi, M. E. Itkis, and R. C. Haddon, "Soluble graphene derived from graphite fluoride," *Chemical Physics Letters,* vol. 445, pp. 51-56, Sep 2007.

[42] S. Niyogi, E. Bekyarova, M. E. Itkis, J. L. McWilliams, M. A. Hamon, and R. C. Haddon, "Solution properties of graphite and graphene," *Journal of the American Chemical Society,* vol. 128, pp. 7720-7721, Jun 2006.

[43] S. Stankovich, R. D. Piner, S. T. Nguyen, and R. S. Ruoff, "Synthesis and exfoliation of isocyanate-treated graphene oxide nanoplatelets," *Carbon,* vol. 44, pp. 3342-3347, Dec 2006.

[44] D.-D. Zhang, S.-Z. Zu, and B.-H. Han, "Inorganic-organic hybrid porous materials based on graphite oxide sheets," *Carbon,* vol. 47, pp. 2993-3000, 2009.

[45] D. C. Elias, R. R. Nair, T. M. G. Mohiuddin, S. V. Morozov, P. Blake, M. P. Halsall*, et al.*, "Control of Graphene's Properties by Reversible Hydrogenation: Evidence for Graphane," *Science,* vol. 323, pp. 610-613, Jan 2009.

[46] K. Novoselov, "Beyond the wonder material," *Physics World,* vol. 22, pp. 27-30, Aug 2009.

[47] J. R. Potts, D. R. Dreyer, C. W. Bielawski, and R. S. Ruoff, "Graphene-based polymer nanocomposites," *Polymer,* vol. 52, pp. 5-25, Jan 2011.

[48] S. Ashley, "Artificial muscles (electroactive polymers, EAP)," *Scientific American,* vol. 289, pp. 52-59, 2003.

[49] X. D. Lou, R. Daussin, S. Cuenot, A. S. Duwez, C. Pagnoulle, C. Detrembleur*, et al.*, "Synthesis of pyrene-containing polymers and noncovalent sidewall functionalization of multiwalled carbon nanotubes," *Chemistry of Materials,* vol. 16, pp. 4005-4011, Oct 19 2004.

[50] M. Matsuoka, M. Yamamoto, K. Adachi, Y. Tsukahara, and T. Konno, "Dispersion Behavior of Multi-walled Carbon Nanotubes with Pyrene-Containing Linear and Graft Polymers as Non-covalent Surface Modifiers," *Designed Monomers and Polymers,* vol. 13, pp. 387-397, 2010.

[51] S. Meuer, L. Braun, and R. Zentel, "Pyrene Containing Polymers for the Non-Covalent Functionalization of Carbon Nanotubes," *Macromolecular Chemistry and Physics,* vol. 210, pp. 1528-1535, Sep 22 2009.

[52] P. Petrov, F. Stassin, C. Pagnoulle, and R. Jerome, "Noncovalent functionalization of multi-walled carbon nanotubes by pyrene containing polymers," *Chemical Communications,* pp. 2904-2905, 2003.

[53] Y. Ji, Y. Y. Huang, A. R. Tajbakhsh, and E. M. Terentjev, "Polysiloxane Surfactants for the Dispersion of Carbon Nanotubes in Nonpolar Organic Solvents," *Langmuir,* vol. 25, pp. 12325-12331, Oct 20 2009.

[54] L. L. Ji, W. Chen, L. Duan, and D. Q. Zhu, "Mechanisms for strong adsorption of tetracycline to carbon nanotubes: A comparative study using activated carbon and graphite as adsorbents," *Environmental Science & Technology,* vol. 43, pp. 2322-2327, Apr 2009.

[55] J. Q. Liu, L. Tao, W. R. Yang, D. Li, C. Boyer, R. Wuhrer*, et al.*, "Synthesis, Characterization, and Multilayer Assembly of pH Sensitive Graphene-Polymer Nanocomposites," *Langmuir,* vol. 26, pp. 10068-10075, Jun 2010.

[56] J. Q. Liu, W. R. Yang, L. Tao, D. Li, C. Boyer, and T. P. Davis, "Thermosensitive Graphene Nanocomposites Formed Using Pyrene-Terminal Polymers Made by RAFT Polymerization," *Journal of Polymer Science Part a-Polymer Chemistry,* vol. 48, pp. 425-433, Jan 2010.

[57] M. Molberg, D. Crespy, P. Rupper, F. Nuesch, J. A. E. Manson, C. Lowe*, et al.*, "High Breakdown Field Dielectric Elastomer Actuators Using Encapsulated Polyaniline as High Dielectric Constant Filler," *Advanced Functional Materials,* vol. 20, pp. 3280-3291, Oct 2010.

[58] D. C. Marcano, D. V. Kosynkin, J. M. Berlin, A. Sinitskii, Z. Z. Sun, A. Slesarev*, et al.*, "Improved Synthesis of Graphene Oxide," *Acs Nano,* vol. 4, pp. 4806-4814, Aug 2010.

[59] S. Stankovich, D. A. Dikin, R. D. Piner, K. A. Kohlhaas, A. Kleinhammes, Y. Jia*, et al.*, "Synthesis of graphene-based nanosheets via chemical reduction of exfoliated graphite oxide," *Carbon,* vol. 45, pp. 1558-1565, Jun 2007.

[60] S. Michel, X. Q. Q. Zhang, M. Wissler, C. Lowe, and G. Kovacs, "A comparison between silicone and acrylic elastomers as dielectric materials in electroactive polymer actuators," *Polymer International,* vol. 59, pp. 391-399, Mar 2010.

[61] F. K. Tuinstra, J. L., "Raman Spectrum of Graphite," *Journal of Chemical Physics,* vol. 53, pp. 1126-1130, 1970.

[62] K. N. Kudin, B. Ozbas, H. C. Schniepp, R. K. Prud'homme, I. A. Aksay, and R. Car, "Raman spectra of graphite oxide and functionalized graphene sheets," *Nano Letters,* vol. 8, pp. 36-41, Jan 2008.

[63] Y. W. Long, J.; Lv, Y.; Tao, C.; Xia, L.; Zhu, H., "Preparation and Characterization of Graphene by the Oxidation Reduction Method," *Advanced Materials Research,* vol. 554 - 556, pp. 624-627, 2012.

[64] P. Xiao, M. Xiao, and K. C. Gong, "Preparation of exfoliated graphite/polystyrene composite by polymerization-filling technique," *Polymer,* vol. 42, pp. 4813-4816, May 2001.

[65] G. M. Tsangaris, G. C. Psarras, and N. Kouloumbi, "Evaluation of dielectric behaviour of particulate composites consisting of polymeric matrix and conductive filler," *Materials Science and Technology,* vol. 12, pp. 533-538, Jul 1996.

[66] C. Brosseau, P. Queffelec, and P. Talbot, "Microwave characterization of filled polymers," *Journal of Applied Physics,* vol. 89, pp. 4532-4540, Apr 15 2001.

[67] G. M. Tsangaris, G. C. Psarras, and N. Kouloumbi, "Electric modulus and interfacial polarization in composite polymeric systems," *Journal of Materials Science,* vol. 33, pp. 2027-2037, Apr 15 1998.

[68] D. M. Yu, J. S. Wu, L. M. Zhou, D. R. Xie, and S. Z. Wu, "The dielectric and mechanical properties of a potassium-titanate-whisker-reinforced PP/PA blend," *Composites Science and Technology,* vol. 60, pp. 499-508, 2000.

[69] C. Huang and Q. Zhang, "Enhanced Dielectric and Electromechanical Responses in High Dielectric Constant All-Polymer Percolative Composites," *Advanced Functional Materials,* vol. 14, pp. 501-506, 2004.

[70] P. G. Liu and K. C. Gong, "Synthesis of polyaniline-intercalated graphite oxide by an in situ oxidative polymerization reaction," *Carbon,* vol. 37, pp. 706-707, 1999.

[71] R. Tamura, E. Lim, T. Manaka, and M. Iwamoto, "Analysis of pentacene field effect transistor as a Maxwell-Wagner effect element," *Journal of Applied Physics,* vol. 100, Dec 1 2006.

[72] F. He, S. Lau, H. L. Chan, and J. T. Fan, "High Dielectric Permittivity and Low Percolation Threshold in Nanocomposites Based on Poly(vinylidene fluoride) and Exfoliated Graphite Nanoplates," *Advanced Materials,* vol. 21, pp. 710-+, Feb 9 2009.

[73] P. Fan, L. Wang, J. T. Yang, F. Chen, and M. Q. Zhong, "Graphene/poly(vinylidene fluoride) composites with high dielectric constant and low percolation threshold," *Nanotechnology,* vol. 23, Sep 14 2012.

[74] M. Arbatti, X. B. Shan, and Z. Y. Cheng, "Ceramic-polymer composites with high dielectric constant," *Advanced Materials,* vol. 19, pp. 1369-+, May 21 2007.

[75] Y. P. Sun, K. F. Fu, Y. Lin, and W. J. Huang, "Functionalized carbon nanotubes: Properties and applications," *Accounts of Chemical Research,* vol. 35, pp. 1096-1104, Dec 2002.

[76] C. A. Dyke and J. M. Tour, "Overcoming the insolubility of carbon nanotubes through high degrees of sidewall functionalization," *Chemistry-a European Journal,* vol. 10, pp. 813-817, Feb 20 2004.

[77] D. Tasis, N. Tagmatarchis, V. Georgakilas, and M. Prato, "Soluble carbon nanotubes," *Chemistry-a European Journal,* vol. 9, pp. 4001-4008, Sep 5 2003.

[78] J. W. Shang, Y. H. Zhang, L. Yu, B. Shen, F. Z. Lv, and P. K. Chu, "Fabrication and dielectric properties of oriented polyvinylidene fluoride nanocomposites incorporated with graphene nanosheets," *Materials Chemistry and Physics,* vol. 134, pp. 867-874, Jun 15 2012.

[79] H. Stoyanov, D. Mc Carthy, M. Kollosche, and G. Kofod, "Dielectric properties and electric breakdown strength of a subpercolative composite of carbon black in thermoplastic copolymer," *Applied Physics Letters,* vol. 94, Jun 8 2009.

[80] Y. Tomonari, H. Murakami, and N. Nakashima, "Solubilization of single-walled carbon nanotubes by using polycyclic aromatic ammonium amphiphiles in water - Strategy for the design of high-performance solubilizers," *Chemistry-a European Journal,* vol. 12, pp. 4027-4034, May 15 2006.

[81] S. R. Lu, S. R. Li, J. H. Yu, Z. K. Yuan, and B. Qi, "Epoxy nanocomposites filled with thermotropic liquid crystalline epoxy grafted graphene oxide," *Rsc Advances,* vol. 3, pp. 8915-8923, 2013.

[82] O. Monticelli, S. Bocchini, A. Frache, E. S. Cozza, O. Cavalleri, and L. Prati, "Simple Method for the Preparation of Composites Based on PA6 and Partially Exfoliated Graphite," *Journal of Nanomaterials,* 2012.

[83] C. F. K.-T. A. L. F. J., "Novel Phenolic Resins with Improved Mechanical and Toughness Properties," *Journal of Applied Polymer Science,* vol. 123, pp. 2131-2139, 2012.